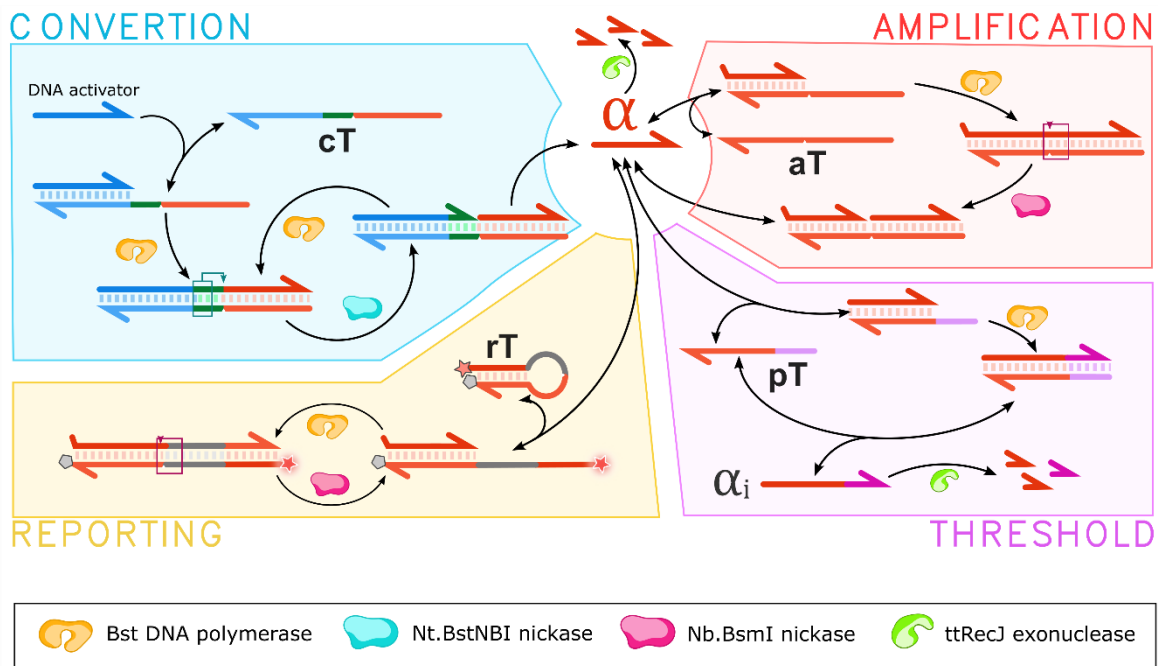
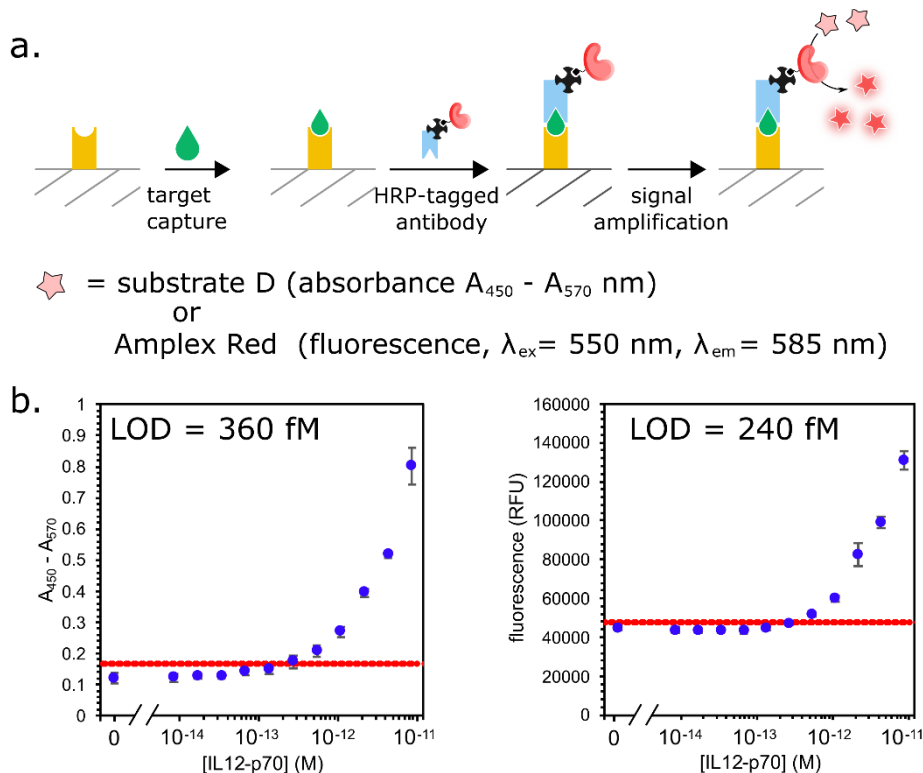


Supplementary Information

Supplementary Figure 1. Detailed PUMA reaction network.....	18
Supplementary Figure 2. ELISA benchmark for the detection of IL-12 p70.	18
Supplementary Figure 3. Demonstration of the leak of the conversion template.	19
Supplementary Figure 4. Antibody specificity for the detection of IL-4, IL-12 and IFN γ	19
Supplementary Figure 5. Optimization of the source template sequence.....	20
Supplementary Figure 6. Effect of the biotin position on the activity of the sT.....	21
Supplementary Figure 7. Specificity of the i-PUMA reaction.	21
Supplementary Figure 8. Biotinylated oligonucleotides exchange and its effect on the classification.	22
Supplementary Figure 9. Testing of the dual biotin-modified source templates.	23
Supplementary Figure 10. Test of different killer templates for negative weight implementation.	23
Supplementary Figure 11. Molecular perceptrons performed at 37 °C.	24
Supplementary Figure 12. Quantification of the detection antibody.	25

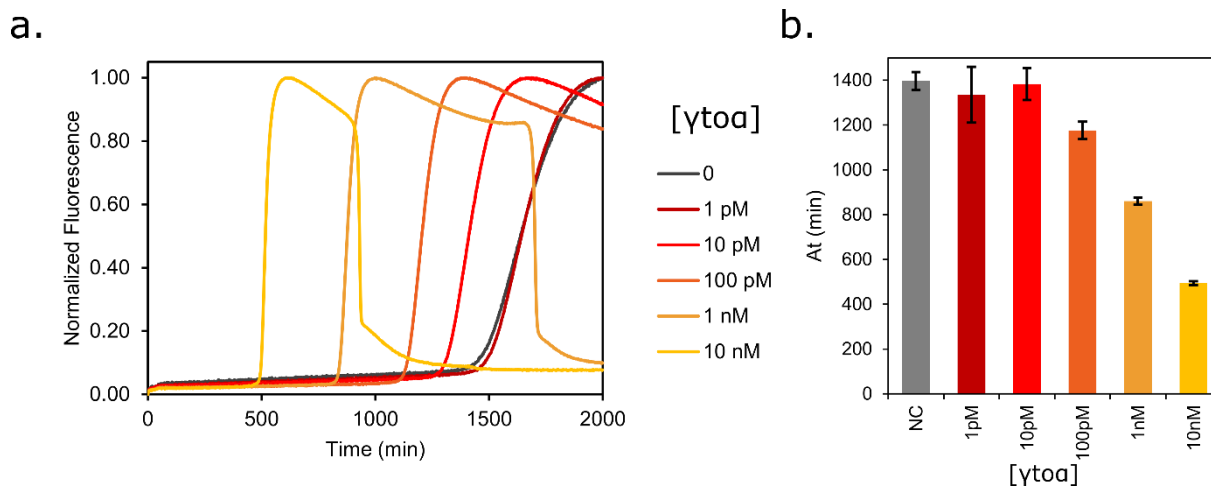


Supplementary Figure 1. Detailed PUMA reaction network. The conversion template (cT) uses the DNA activator as an input primer to produce the α strand output. The autocatalytic template (aT) exponentially replicates α using an exponential amplification reaction mechanism. The pseudotemplate (pT) deactivates α by mediating the addition of a short polynucleotide tail that prevent the product (α_i) to be replicated on the aT. The reporter template (rT) binds to the amplified α to generate a fluorescence used to monitor the amplification reaction. All produced species are dynamically depolymerized into deoxyribonucleosides monophosphate by the exonuclease.

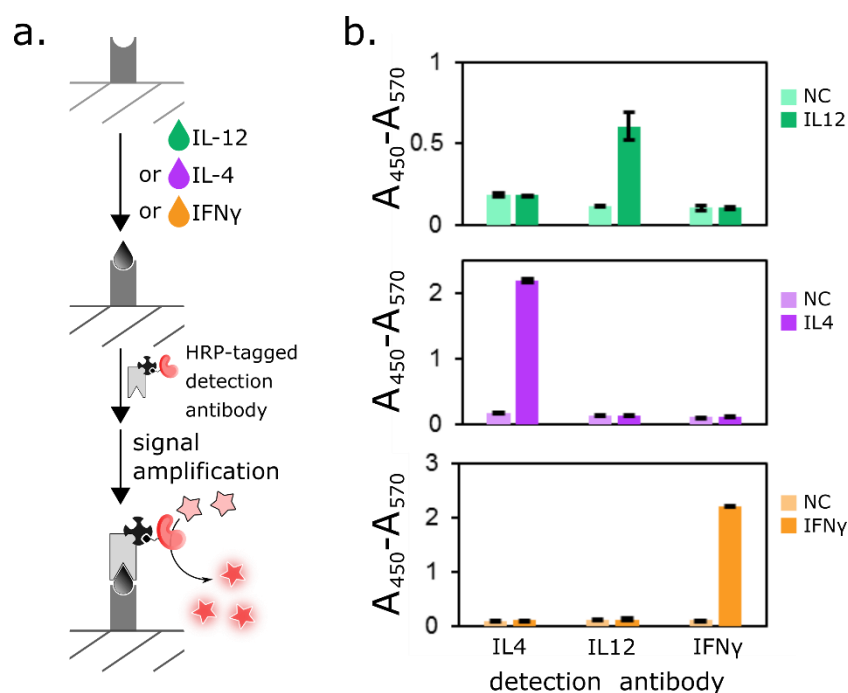


Supplementary Figure 2. ELISA benchmark for the detection of IL-12 p70. **a.** Schematic of the ELISA sandwich assay. The capture antibody (yellow) is physisorbed on a polystyrene well plate and the detection antibody (blue) is

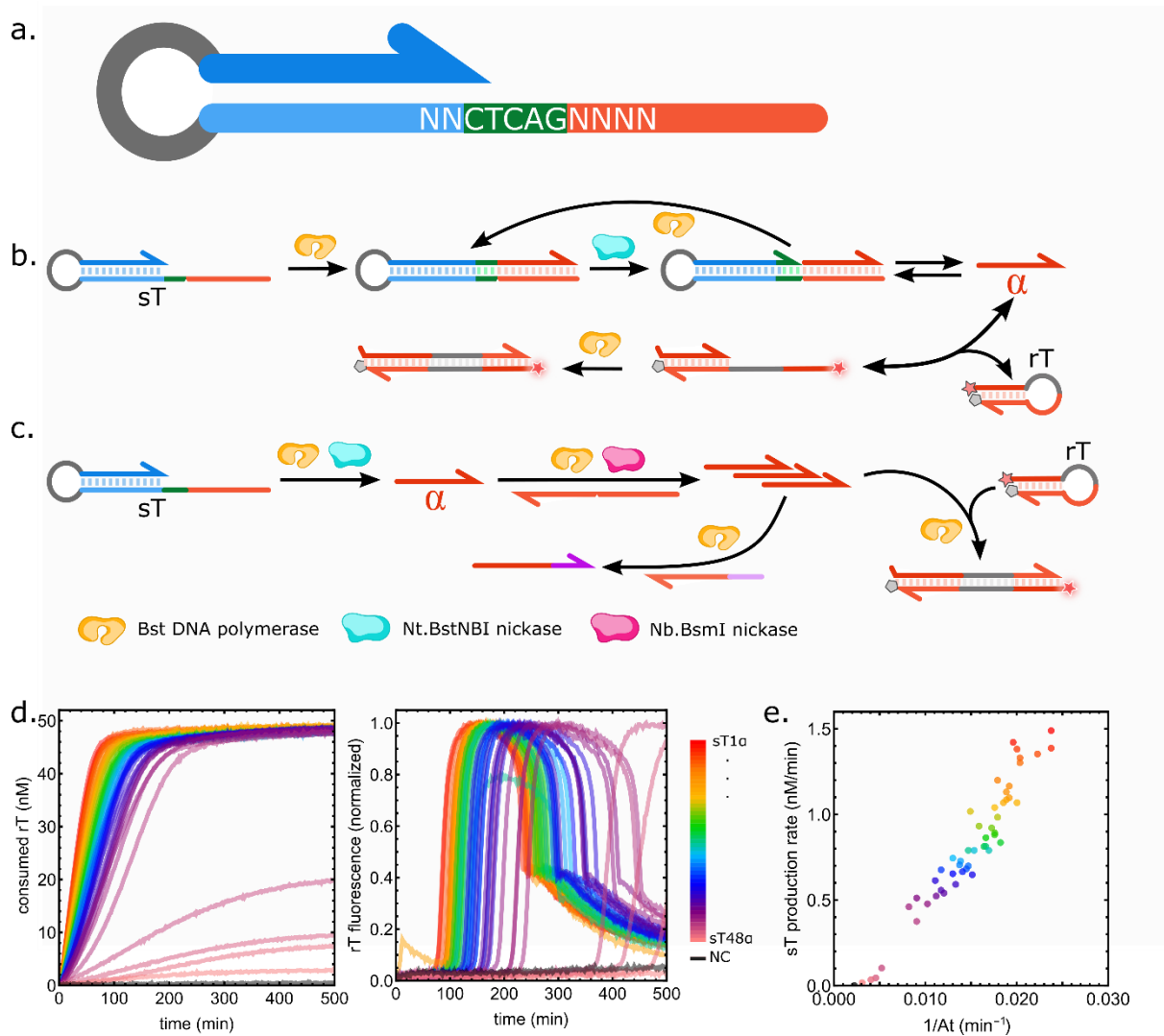
labelled with horseradish peroxidase enzyme. Signal generation is measured either by absorbance using the Substrate D or by fluorescence with the Amplex Red substrate (cf. Material and Method for more details on the protocol). **b.** ELISA assay for the detection of the cytokine IL12-p70 using absorbance (left) or fluorescence readout (right). Error bars correspond to the standard deviation for a triplicate of dilution. The dashed red line corresponds to 3 times the standard deviation of the negative control, used to determine the LoD.



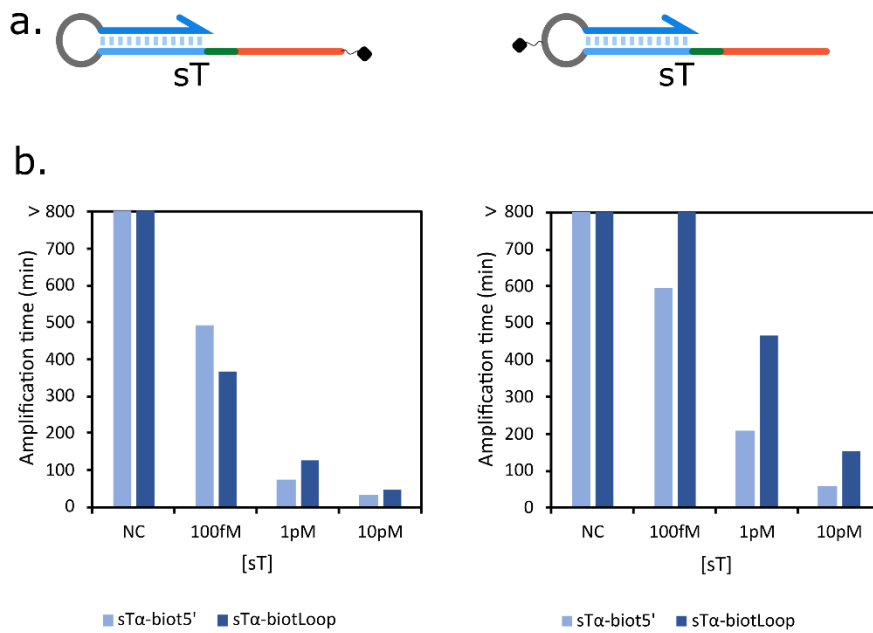
Supplementary Figure 3. Demonstration of the leak of the conversion template. The cT γ_{toa} is incubated at various concentration with the amplification mixture, in absence of the γ input sequence. **a.** Amplification time traces for 1 of the three technical replicates. **b.** Nonspecific amplification time as the function of the cT concentration. We observed that the nonspecific amplification is substantially delayed for cT concentration in the nanomolar range (≥ 1 nM).



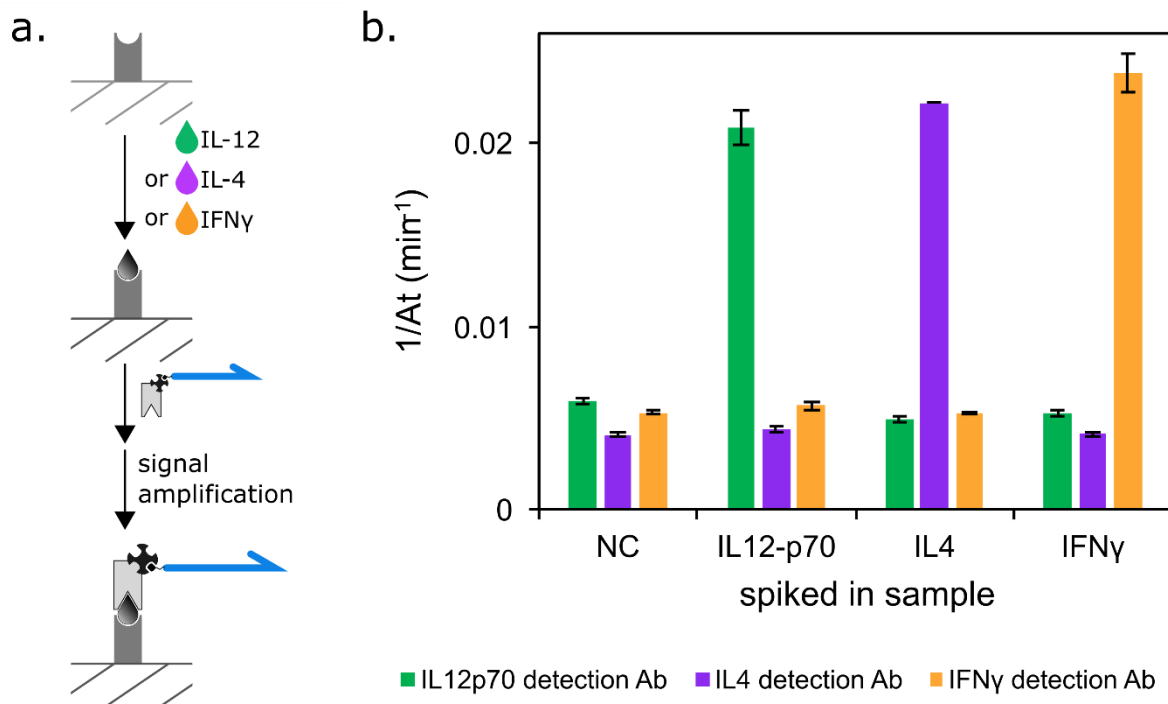
Supplementary Figure 4. Antibody specificity for the detection of IL-4, IL-12 and IFN γ . **a.** Independent ELISA using absorbance readout were conducted in presence or absence of the target using each of the three detection antibodies labelled with HRP. **b.** End-point absorbance signal for a negative control (no target cytokine) and a positive control (8.7 pM IL-12, 8.9 pM IL-4 or 29.6 pM IFN γ). Error bars correspond to the standard deviation for a triplicate of dilution.



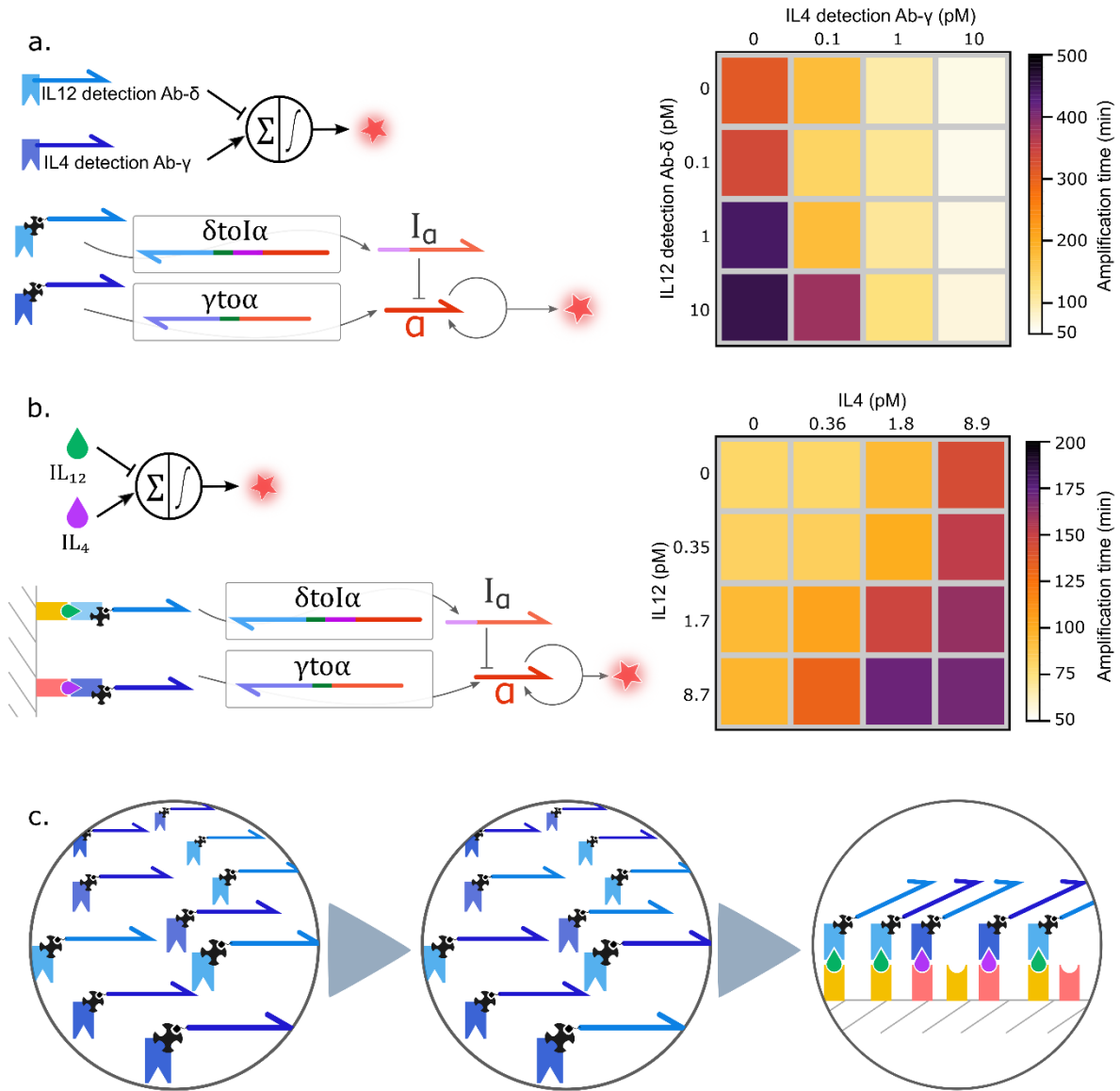
Supplementary Figure 5. Optimization of the source template sequence. **a.** The 2 nucleotides in 3' and the 4 nucleotides in 5' (noted "N") of the Nt.BstNBI nicking enzymes were evaluated with respect to the activity of the source template. 48 out of the 4096 (4^6) random combinations were tested. **b.** The linear production rate of α by the sT (1 nM) was measured by monitoring the direct loading of the rT probe (50 nM), in absence of the exponential amplification module. **c.** Complementarily, the sensitivity of the switch to each sT was estimated by spiking 10 pM of sT in the amplification mixture (aT/rT/pT + enzymes). **d.** Time traces of the linear production rate (left) and exponential amplification reaction (right) for the various tested sT. **e.** sT production rate as a function of the sT triggering efficacy (as $1/At$).



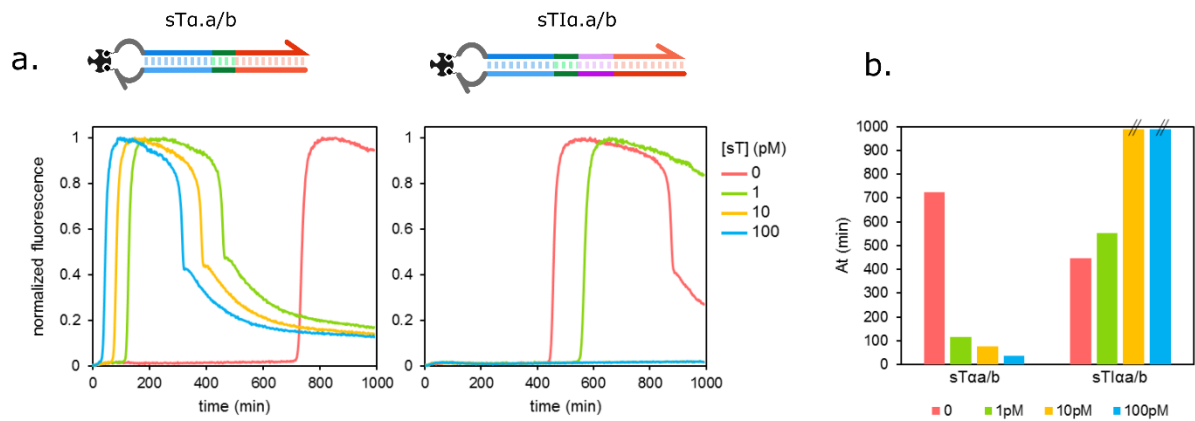
Supplementary Figure 6. Effect of the biotin position on the activity of the sT. **a.** The biotin moiety has been introduced either at the 5' extremity via a hexaethylene glycol spacer (sp18, Biomers) followed by a pentathymidylate linker (left) or internal to the loop by post-conjugation of an amino-dT building block (right). **b.** Amplification time of samples spiked with a varying concentration of sT in absence (left) or presence (right) of streptavidin (sT/STp 4:1).



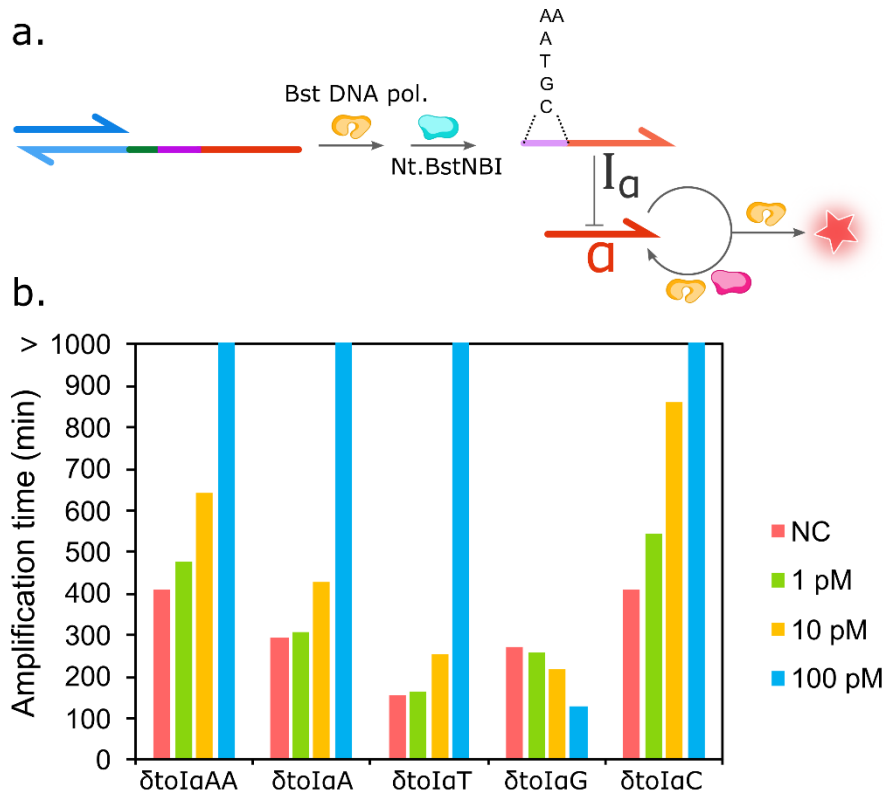
Supplementary Figure 7. Specificity of the i-PUMA reaction. **a.** Each i-PUMA assay uses the cognate pair of capture and sT-tagged detection antibodies. The capture step is performed on a sample containing one of the 3 cytokines (8.7 pM IL-12, 8.9 pM IL-4 or 29.6 pM IFN γ). **b.** Amplification times for the different samples (plotted as 1/At) show an exquisite selectivity for each of the targeted proteins.



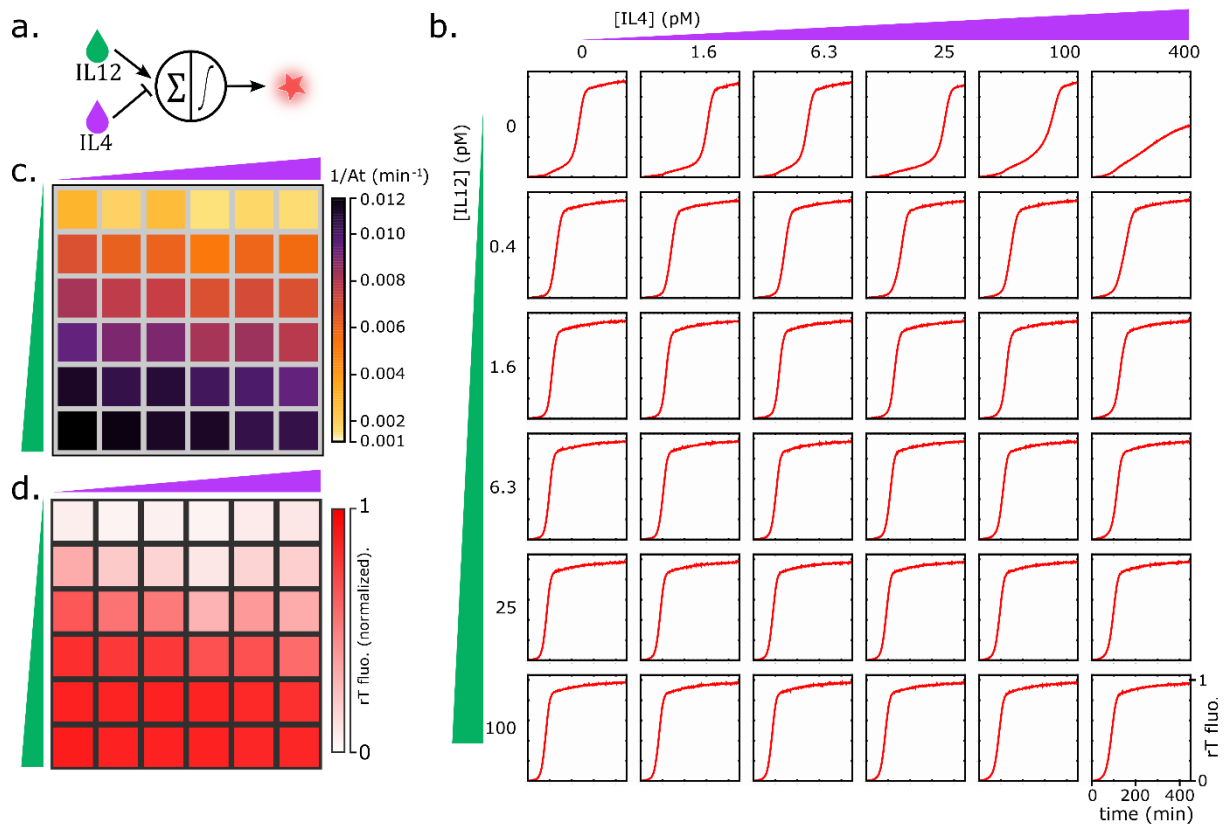
Supplementary Figure 8. Biotinylated oligonucleotides exchange and its effect on the classification. **a.** Initial protein classifiers were realized using oligonucleotide inputs conjugated to the detection antibodies and the corresponding templates added in solution in the amplification mixture. To demonstrate the classification capabilities of this strategy, we first tested the classifier using various concentrations of DNA input-grafted antibodies (IL12 and IL4 detection antibodies functionalized with the oligonucleotide δ and γ and associated with the positive weight converter template $\delta\text{to}\alpha$ and negative weight killer template $\gamma\text{to}\alpha$, respectively, cf. Supplementary Material). The array plot demonstrates the proper response of the switch depending on both IL12 and IL4 detection antibodies, which respectively delays and accelerates the time of amplification. **b.** Using the same set of detection antibodies and templates, we tested the classifier on the two targeted cytokines. A fixed concentration of DNA input-grafted antibodies is incubated with the target proteins captured on a support, prior to incubation with the amplification mixture. The array plot reveals that the amplification time is delayed by the presence of IL12, although with a milder effect as compared to when the antibodies are directly injected in the amplification mixture at various concentrations (**a.**). However, the same effect is observed in the IL4 dimension, while this cytokine is supposed to activate the α switch. **c.** These observations suggest that the biotinylated DNA inputs are able to switch antibody^{69–71}, which results in cytokines being associated with the incorrect DNA input, eventually distorting the classification.



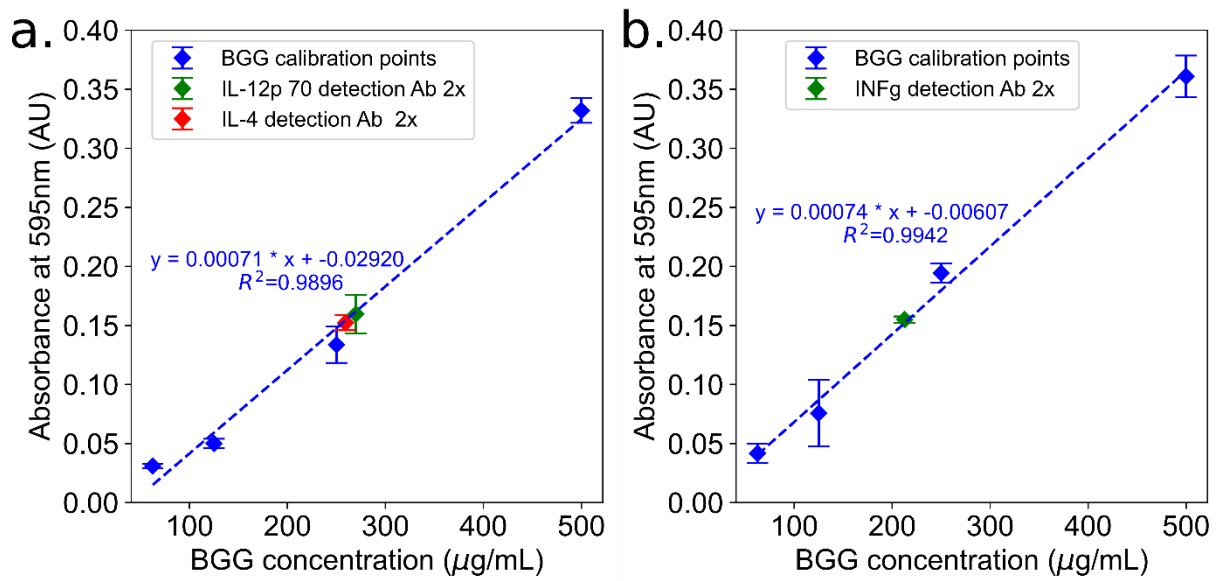
Supplementary Figure 9. Testing of the dual biotin-modified source templates. The amplification mixture is spiked with varying concentration of sT α .a/sT α .b or sTII α .a/sTII α .b and the amplification reaction is recorded in real-time. **a.** Amplification curves in presence of sT α .a/sT α .b (left, [pT α] = 10 nM) or sTII α .a/sTII α .b (right, [pT α] = 7 nM). **b.** As expected, the amplification time is respectively lower and higher as sT α .a/b and sTII α .a/b is increased.



Supplementary Figure 10. Test of different killer templates for negative weight implementation. **a.** A killer template δ toI α loaded with the activator strand δ produces I α under polymerization/nicking cycles. I α hybridizes to α triggers and mediates their deactivation by extension along the template's tail (in pink). Various tail extensions were tested in presence of the amplification switch, 2.5 nM of δ toI α and a varying concentration of δ . **b.** Amplification times for the different kT extensions (double nucleotide AA or single nucleotide A, T, G or C). Because of its efficient inhibitory effect (even from 1 pM of input DNA), the sequence of the δ toI α C was selected to implement negative weights. As for the optimization of source template in the context of molecular perceptron, this sequence was adapted to a bis-biotinylated design (sequences sTII α .a-biot5' and sTII α .b-biot3', cf. Supplementary Material). Such design allows to wash off the excess of kT after the capture step (mitigating the leakage effect), and stabilizes its interaction with the cognate streptavidin-modified antibody (limiting the exchange with sT-grafted antibody during the capture step, Supplementary Figure 9)



Supplementary Figure 11. Molecular perceptrons performed at 37 °C. **a.** IL4 (negative weight) and IL12 (positive weight) was implemented using the β amplification switch and bis-biotinylated sT and kT tagging respectively the IL12 and IL4 detection antibody. **b.** Normalized fluorescence time traces for various concentrations of the two input proteins. **c.** Array plot of the 2D input space color-coded as a function of the amplification time. **d.** Molecular perceptron output fluorescence at 120 minutes of incubation. The more graded response as compared to the molecular perceptrons operating at 50°C (Figures 3-4), can be attributed to the slight linear fluorescence increase prior to the exponential amplification phase. Such linear amplification can be explained by the direct loading of the probe with the output of the source template, a phenomenon that is more favorable at 37 °C than at 50 °C.



Supplementary Figure 12. Quantification of the detection antibody. **a.** A Bradford calibration curve (blue) has been realized with Bovine Gamma Globulin (BGG) allowing to determine the 2x stock concentration of the commercial IL-12 p70 detection Ab (green, 270 µg/mL, i.e. 1.80 µM, assuming a 150 kDa MW) and of the IL-4 detection Ab (red, 259 µg/mL, i.e. 1.73 µM). **b.** A Bradford calibration curve (blue) has been realized with BGG to quantify the INFγ detection Ab (green, 213 µg/mL, i.e. 1.42 µM). Error bars correspond to the standard deviation on three dilution triplicates.